PHOTOMETRY OF THE SATURNIAN SATELLITES DURING RING PLANE CROSSING

B. J. Buratti and J. A. Mosher
Palomar Observatory and Jet Propulsion Laboratory
California Institute of Technology
4800 Oak Grove Dr.
Mail Code 183-501
Pasadena, CA 91109
(818)354-7427
FAX (818)354-0966
bonnie.buratti@jpl.nasa.gov

P. D. Nicholson and C. A. McGhee
Palomar Observatory and Cornell University
Department of Astronomy
Ithaca, NY 14853

R. G. French[*]
Wellesey College
Department of Astronomy
Wellesley, MA 02181

25 manuscript pages
7 figures

[*]Guest Observer, Palomar Mountain Observatory

ABSTRACT

Photometric observations of the five medium-sized satellites of Saturn were obtained with the 60-inch telescope at Palomar Mountain Observatory during the Ring Plane Crossing in August 1995. The albedos of these satellites are very high at ~0.9 μm, an indication that the fraction of opaque contaminants on their surfaces is very low. The geometric albedos for the leading sides of the satellites are: Enceladus: 1.02; Tethys: 0.90; Dione: 0.72; and Rhea: 0.76. For Mimas, the geometric albedo of the trailing side is 0.72. The amplitudes of the satellites' rotational lightcurves is somewhat less than in the visual portion of the spectrum, ranging from 0.40 for Dione to 0.10 for Rhea, to 0.05 for Tethys. The lightcurve of Enceladus is not sinusoidal. Both Enceladus and Mimas are brighter on the trailing side, unlike the other three satellites. This result suggests that coating by Saturn's E-ring is a major factor in determining the optical properties of all five satellites.

I. Introduction

The reduction of glare from Saturn's rings during the occasions that they appear edge-on from Earth affords a rare opportunity to observe the inner satellites of Saturn. Groundbased photometric observations of Mimas and Enceladus, the faintest two of the five medium-sized inner satellites of Saturn, can be reliably obtained only during these ring plane crossings (RPXs), which occur about once every 15 years. Indeed, William Herschel discovered these two satellites during a previous RPX in 1789. The episode of RPXs that occurred in 1995-1996 is the best until 2038.

In this paper we report on the analysis of nearly 300 images obtained during August 9-12 August 1995 (the actual crossing was on August 10 at 20:54 UT, in daylight). These observations provide important new information on the rotational lightcurves and geometric albedos of all five inner medium satellites: Mimas, Enceladus, Tethys, Rhea, and Dione (see Table 1 for a summary of their physical properties). The rotational lightcurves can be used to understand the distribution of geologic terrains on the satellites, and to understand the effects of various exogenic alteration processes, including the accretion of E-ring particles onto the satellites (Buratti et.al, 1990; Hamilton and Burns, 1993; and Verbiscer and Veverka, 1992). These measurements are especially important for the areas of the satellites that were not imaged by the Voyager spacecraft.

To reduce scattered light from Saturn itself, and to reduce

moonlight (the observations were obtained in light time), the bulk of our observations were obtained in the methane absorption band at 0.89 μm. We utilized a narrow band interference filter provided by Prof. James Westphal of Caltech, with an effective wavelength of 0.889 μm and a FWHM of 50 μm. Our measurements of the lightcurves and geometric albedos of these bodies at this wavelength are the first in the near infrared. Previous groundbased and Voyager observations were limited to the visual region extending only to 0.75 μm (Noland et al., 1974, Franz and Millis, 1975, Buratti and Veverka, 1984, Verbiscer and Veverka, 1992). Quantitative measurements in this new region of the spectrum are important to set the context for observations by the Cassini spacecraft, which includes a suite of optical and infrared remote sensing instruments (Space Science Reviews, in preparation).

II. Observations and Data Analysis

The observations were obtained with the 60-inch telescope at Palomar Mountain Observatory with a 1024 X 1024 CCD array camera at the Cassegrain focus. A summary of our observations is listed in Table 2. Good weather and fair seeing persisted throughout the four nights; the worst seeing of ~ two arc seconds occurred near dawn. There was a full moon on August 11, located about 27° away from the Saturnian system. Integration times were nominally two minutes. An image near the actual Ring Plane Crossing is shown in Figure 1. Landolt standard star fields were imaged throughout the

4

night to obtain absolute photometric measurements on the satellites, including geometric albedos. Flatfield images were obtained by flooding the inside of the dome with an incandescent lamp and acquiring counts to about half of the CCD's full well.

The analysis proceeded following methods we developed previously for performing relative photometry with CCD images. (Buratti and Dunbar, 1991; Buratti et al., 1995). Each image was bias-subtracted and flatfielded, and aperture photometry was performed on each satellite and Titan, which we used for an on-chip comparison standard. Due to the significant amount of scattered light from Saturn still existing on our images, we modeled the "sky" background as a two-dimensional polynomial surface. This technique previously proved successful with our photometric analysis of the Uranian satellites (Buratti et al., 1992). In some cases, two to five images were coadded to increase signal, particularly for Mimas and Enceladus. Absolute photometry of the satellites was obtained with observations of stars in two Landoldt fields (Landoldt, 1992).

No corrections for the orbital lightcurve of Titan were made in our data reductions. Although no rotational light curve of Titan exists in the ~ 0.9 μm region, observations by Noland et al. (1974) between 0.35 and 0.75 μm show no observable rotational light curve amplitude greater than 0.02 magnitudes. Lemmon et al. (1995) and Coustenis et al. (1995) obtained a lightcurve at ~1.1 μm, in a deeper methane absorption band, showing variations of a few percent over Titan's surface. For the ranges of orbital

longitude covered during the four nights of our observations (237°
to 309° degrees), the 1.1 μm data show Titan's rotational curve
exhibits no measurable variations over the period spanned by our
first two nights of observations. For the orbital phases covered
during our third night, Coustenis et al. report a 2% change, while
Lemmon et al. report a 0.5% change. For the fourth night,
Coustenis et al. report a 3% change, and Lemmon et al. report a
1.5% change. Our own comparisons of Titan's integrated brightness
with respect to our standard fields shows no systematic change
greater than 1%. Thus, we decided not to adopt a correction for
Titans' orbital phase curve.

The range in subobserver longitude varies with each satellite;
in general the outer satellites have wider ranges because the four
night period over which we observed spans a wider range in orbital
phase angles (see Table 2). Unfortunately, the orbital period of
Mimas is close to 24 hours (21 hours), so that the satellite
appeared in nearly the same position night after night.
Nevertheless, we observed Mimas for a range of 30 degrees not
observed by the Voyager spacecraft. The solar phase angle during
the four nights changed from 3.7 to 3.5; this is not a sufficient
change to obtain any information on the satellites' phase
functions. The change is so small that corrections for solar phase
effects are not necessary (they are expected to be a fraction of a
percent; see Buratti and Veverka, 1984).

The relative photometric error for the four nights is 1-2%.
Observations of the same rotational phases for Enceladus, Mimas and

Tethys on different nights are consistent to that level. The major source of relative error is scattered light from Saturn. We estimate our absolute error to be ~5%, based on the differences in the derived geometric albedos from various Landoldt field stars, and uncertainties in the radii of the satellites and in the magnitude of the Sun.

III. Geometric albedos

To obtain a geometric albedo for each satellite, the integrated brightness was first converted to a magnitude scale through the Landoldt standard star magnitudes. These observed magnitudes, $m_{S(obs)}$, were then converted to opposition magnitudes, $m_{S(opp)}$ for each satellite with the following equation:

$$m_{S(opp)} = m_{S(obs)} - \alpha\beta \qquad (1)$$

where α is the solar phase angle and β is the phase coefficient measured in magnitudes/degree. Ideally, phase coefficients over the same range in solar phase angle should be used for this computation. These phase coefficients do exist from previous groundbased measurements for Tethys, Dione, and Rhea (Noland, 1974; Franz and Millis, 1975), whereas for the cases of Mimas and Enceladus, the Voyager phase coefficients obtained at larger phase angles were used (Buratti and Veverka, 1984; the Voyager phase coefficient was also used for Dione, because the Noland et al. and

7

Franz and Millis results are very different). There is a slight wavelength dependence to the phase coefficient: in general, as the albedo increases the phase coefficient decreases (Noland et al., 1974). Because there is no strong change in albedo between 0.50 and 0.90 μm (see Figure 2), our adoption of a phase coefficient derived at shorter wavelengths does not introduce a significant error. The adopted phase coefficients are listed in Table 3.

The geometric albedo for each satellite was then computed with the following equation:

$$p = \frac{D^2 d^2}{R^2 r^2} 10^{-(m_{s(opp)} + m_\odot)/2.5}$$ (2)

where D is the heliocentric distance of Saturn on the day of the observation, d is the corresponding geocentric distance of Saturn, R is the radius of the satellite (Table 1), $m_\odot$ is the magnitude of the Sun (Allen, 1976). The geometric parameters were obtained from the Jet Propulsion Laboratory's online ephemeris site (ssd.jpl.nasa.gov 6775). The specific images used to obtain the satellites' geometric albedos varied for each object. Images were chosen to optimize the following factors: the visibility of the satellite, the minimization of scattered light from Saturn, the availability of Landolt star images at the same airmass, and the best photometric conditions (seeing, weather, and minimal airmass and moonlight). The best conditions existed for each satellite at the following times: Mimas, Tethys, and Enceladus: August 9, 10:54-11:10 UT; Dione: August 10, 8:14-9:18 UT; and Mimas, Tethys,

8

Rhea and Dione: August 11, 7:51-7:58 UT. Finally, the geometric albedos for both the leading and trailing hemispheres were computed based on the rotational light curves observed for each satellite, and their best-fit sinusoidal curves (see next section). There was not enough rotational phase coverage for Mimas to obtain a geometric albedo for its leading hemisphere. The results are listed in Table 3. The geometric albedo of Titan obtained with the Landoldt comparison stars is 0.086 ± 0.001, in good agreement with the previous value of 0.085 of Neff et al. (1984).

Figure 2 shows the geometric albedos of the satellites with visible geometric albedos (0.35-0.59 μm) determined by the imaging experiment on the Voyager 1 and 2 spacecraft (Buratti and Veverka, 1984). Our results show that the high geometric albedos of the satellites persist to at least ~0.9 μm. Previous spectra of Tethys, Dione, and Rhea (presented on a relative scale) disagreed on whether the albedo of these satellites increased or decreased between 0.6 and 0.9 μm. McCord et al. (1971) and Clark and Owensby (the latter observed Rhea only) show a ~10% decrease, while Fink et al. (1976) show an indeterminate increase. The 10-15% absolute photometric error of Voyager measurements, coupled with our own 5% absolute error, render it impossible to resolve the disagreement.

Due to scattered light from Saturn, so visible spectra of Enceladus or Mimas have been obtained from the ground.

9

IV. Rotational Light Curves

The rotational lightcurve in astronomical magnitudes was derived for each satellite with the following equation:

$$\Delta m(\theta) = 2.5 \log (<B>/B(\theta)) \qquad (3)$$

where θ is the satellite's orbital longitude, measured in the prograde direction from superior conjunction, B is the integrated brightness with respect to Titan, and $<B>$ is the mean brightness. For Tethys, Dione, and Rhea, the data were fit to the following two-parameter equation:

$$\Delta m(\theta) = A/2[\cos(\theta - \theta_0)] \qquad (4)$$

where A is the peak to peak amplitude of the variation and θ_0 is the longitude at which the peak brightness occurs. For Mimas, there was insufficient orbital phase coverage to fit a sinusoidal curve; Voyager imaging observations were merged with our data to derive the sinusoidal fit shown in Figure 3. For Enceladus, the albedo variegations do not appear to follow a sinusoidal distribution. The results for each satellite are listed in Table 4 and shown in Figures 3 to 7. The figures include previous measurements from ground based and Voyager measurements (Noland et al., 1974; Franz and Millis, 1975; Buratti and Veverka, 1984 Verbiscer and Veverka, 1992).

10

In general the rotational light curves for the three outer medium sized satellites follow the previously observed pattern of brighter leading hemispheres. Our observations show clearly that the trailing side of Enceladus is brighter than the leading side. Both ground-based (Franz and Millis, 1975) and Voyager measurements (Buratti and Veverka, 1984) suggested that the global albedo variegations on Enceladus were different than those on other satellites; however, none of the previous data were good enough to show the pattern unambiguously (see Figure 4). If our observations of Mimas are combined with the Voyager data, we confirm the result of Verbiscer and Veverka (1992) that its trailing side is also slightly brighter than its leading side.

V. Discussion

The medium sized Saturnian satellites occupy a unique place among satellites: in the near UV and visible portion of the spectrum they are far brighter than any other class of objects in the solar system (Buratti and Veverka, 1984; Nelson and Lane 1987). This high albedo implies a surface consisting of nearly fresh ice with very little opaque contaminants. Our results from Saturn Ring Plane Crossing show that this high albedo persists into the near IR (~0.9 μm). Laboratory measurements by Clark (1981) show that a tiny amount of dark, opaque contaminant (silicate or charcoal) reduces the albedo of a frost surface drastically. For example, a mineral coverage of only 0.002 % results in a decrease in albedo

11

from 0.97 to 0.89.   This remarkably uncontaminated ice implies relatively recent activity in the Saturnian system.   However, crater counting studies from Voyager images have shown the geologic age of most of the satellites' terrains to date from the end of the period of heavy bombardment, except for the most recent terrains on Enceladus, which are less than 200 million years old (Plescia and Boyce, 1985). Thus, the activity must in general be a surficial (exogenic) process.

Our lightcurves in this spectral region exhibit better signal to noise than previous studies (although our phase coverage is not as extensive in some cases).   For Tethys, Dione, and Rhea our results are consistent with previous work in the visual range. Our full amplitudes appear to be slightly less than those in that spectral range (see Figures 3 through 7).   This result would be consistent with a decreased contrast between ices and opaque material in the near IR.

We find a general pattern in the leading/trailing dichotomies observed in the inner Saturnian system: those satellites exterior to the densest point in the E-ring have brighter leading sides, while those interior to its densest point (including Enceladus) have brighter trailing sides.   This is the prediction made by Hamilton and Burns (1994) in their paper on the dynamics of Saturn's E-ring. Although other mechanisms such as micrometeoritic and magnetospheric bombardment can brighten (darken) the leading (trailing) hemisphere (see Buratti, Mosher and Johnson, 1990 for a more extensive discussion), the overall pattern seen among the five

satellites suggests that the E Ring is the dominant factor in determining their optical properties.

The E Ring is a tenuous distended structure spanning the region between 3 and 8 Saturnian radii; it appears to consist of micron-sized ice particles (Baum et al., 1981; Larson et al., 1981; Seidelmann et al., Showalter et al., 1991; Horyani et al., 1992; Hamilton and Burns, 1994; and Bauer et al., 1997). The location of its optically thickest region near Enceladus strongly suggests a link to that satellite. That some areas of Enceladus are free of craters (Smith et al., 1981) suggests it is geologically active and may thus be the source for the E-ring. Models for the melting of Enceladus include tidal heating (Lissauer et al., 1984; Ross and Schubert, 1989) and the lowering of its melting point due to the presence of NH_3 (Stevenson, 1982). Herkenhoff and Stevenson (1984) present a model for the formation of the E-ring in which liquid extruded onto the surface of Enceladus evaporates and nucleates. Given its size (R=249 km) and low density (1.2 gm/cm3), which implies a primarily icy composition with only small amounts of siliceous material, a melted interior is only marginally likely. This problem led to another model depicting the E-ring as a self-sustaining entity (Hamilton and Burns, 1994). Whatever the mechanism for the ring's creation, the high albedos and general albedo pattern seen on the satellites suggests it alters the surfaces of the five inner medium sized satellites by an ongoing process.

One final point is that the location of Enceladus in the midst

13

of the E ring means it should have no albedo variegations at all. Its trailing side is, however, measurably brighter (see Figure 4). There is thus the indication that if there are currently geologically active (brighter) regions on Enceladus, they will be found on the trailing side. The "recent" terrains imaged by Voyager do in fact appear on this hemisphere (Smith et al., 1982), although no high resolution observations of the leading hemisphere exist. Moreover, the brightest feature on Enceladus is in the southern (poorly imaged) trailing hemisphere. This was the same region measured in the telescopic observations of Franz and Millis (1975), which show a large (0.3 magnitude; see Figure 4) increase in brightness. These data were obtained at a subobserver latitude of -26 degrees, while the Voyager high resolution images were obtained at ~30-45 degrees latitude (our own observations were of course very close to Enceladus's equator). The non-sinusoidal variegations on Enceladus would be consistent with a globally uniform satellite, with a higher albedo, more recent geologic terrain in the southern region of the trailing hemisphere.

Acknowledgements

under contract to the National Aeronautics and Space Administration.

References

Allen, C. W. 1976. Astrophysical Quantities. Athlone Press, London.

Bauer, J., J. J. Lissauer, M. Simon 1997. Edge-on observations of Saturn's E and G rings in the near-IR. Icarus **125**, 440-445.

Baum, W. A., T. Kreidl, J. A. Westphal, G. E. Danielson, P. K. Seidelmann, D. Pascu, and D. G. Currie 1981. Saturn's E-ring, I, CCD observations of March 1980. Icarus **47**, 84-96.

Buratti, B. J., and R. S. Dunbar 1991. Observation of a rapid increase in the brightness of the coma of Comet 2060 Chiron in 1990. Ap. J. **366**, L47-49.

Buratti, B. J., R. S. Dunbar, E. F. Tedesco, J. Gibson, R. L. Marcialis, F. Wong, A. Dobrovolskis, and S. Bennet 1995. Modeling Pluto-Charon mutual events. II CCD observations with the 60-inch telescope at Palomar Mountain. Astron. J. **110**, 1405-1419.

Buratti, B. J., J. Gibson, and J. A. Mosher 1992. CCD Observations of the Uranian satellites. Astron. J. **104**, 1618-1622.

Buratti, B. J., J. A. Mosher, and T. V. Johnson 1990. Albedo and color maps of the Saturnian satellites. Icarus **84**, 339-357.

Buratti B. J., and J. Veverka 1984. Voyager photometry of Rhea, Dione, Tethys, Enceladus, and Mimas. Icarus **58**, 254-264.

Clark, R. N. 1981. The spectral reflectance of water mineral mixtures at low temperatures. J. Geophys. Res. **86**, 3074-3086.

Clark, R. N. and P. D. Owensby 1981. The infrared spectrum of Rhea. Icarus **46**, 354-360.

Coustenis, A., E. Lellouch, J. P. Maillard, and C. P. McKay 1995. Titan's surface: composition and variability from the near-infrared albedo. Icarus **118**, 87-104.

Fink, U., H. P. Larson, T. N. Gautier III, and R. R. Treffers 1976. Infrared spectra of the satellites of Saturn: Identification of water ice on Iapetus, Rhea, Dione, and Tethys. Ap. J. **207**, L63-L67.

Franz, O. G., and R. L. Millis 1975. Photometry of Dione, Tethys, and Enceladus on the UBV system. Icarus **24**, 433-442.

Hamilton, D. P., and J. A. Burns 1994. Origin of Saturn's E ring:

Self-sustained, naturally. Science **264**, 550-553.

Herkenhoff, K. E., and Stevenson, D. J. 1984. Formation of Saturn's
E-ring by evaporation of liquid from the surface of Enceladus.
Lunar Planet. Sci. **15**, 361-362.

Horanyi, M., J. A. Burns, and D. P. Hamilton 1992. The dynamics of
Saturn's E ring particles. Icarus **97**, 248-259.

Landolt, A. U. 1992. UBVRI photometric standard stars in the
magnitude range 11.5 < V < 16.0. Astron. J. **104**, 340-491.

Larson, S. M., J. W. Fountain, B. A. Smith, and H. J. Reitsema
1981. Observations of the Saturn E ring and a new satellite.
Icarus **47**, 288-290.

Lemmon, M. T., E. Karkoschka, and M. Tomasko 1995. Titan's
rotational light-curve. Icarus **113**, 27-38.

Lissauer, J. J., S. J. Peale, and J. N. Cuzzi 1984. Ring torque on
Janus and the melting of Enceladus. Icarus **58**, 159-168.

McCord, T. B., T. V. Johnson, J. H. Elias 1971. Saturn and its
satellites: Narrow band spectrophotometry (0.3-1.1 μm). Ap. J.
165, 413-424.

Neff, J. S., D. C. Humm, J. T. Bergstralh, A. L. Cochran, W. D. Cochran, E. S. Barker, R. O. Tull 1984. Absolute spectrophotometry of Titan, Uranus, and Neptune: 3500-10,500 A. Icarus **60**, 221-225.

Nelson, R. M. and A. L. Lane 1987. Planetary satellites. In Scientific Accomplishments of the IUE (Y. Kondo, Ed.). pp. 67-99. D. Reidel Publishing Co., Boston.

Noland, M., J. Veverka, D. Morrison, D. P. Cruikshank, A. R. Lazarewicz, N. D. Morrison, J. L. Elliot, J. Goguen, and J. A. Burns 1974. Six-color photometry of Iapetus, Titan, Rhea, Dione, and Tethys. Icarus **23**, 334-354.

Plescia, J. B. and Boyce 1985. Impact cratering history of the Saturnian satellites. J. Geophys. Res. **90**, 2029-2037.

Ross, M. N., and G. Schubert 1989. Viscoelastic models of tidal heating in Enceladus. Icarus **78**, 90-101.

Seidelmann, P.K., R. S. Harrington, and V. Szebehely 1984. Dynamics of Saturn's E ring. Icarus **58**, 169-177.

Showalter, M. R., J. N. Cuzzi, S. M. Larson 1991. Structure and particle properties of Saturn's E ring. Icarus **94**, 451-473.

Smith, B. A., and 29 coauthors 1982. A new look at the Saturn
system: the Voyager 2 images. Science **215**, 504-537.

Stevenson, D. J. 1982. Volcanism and igneous processes in small icy
satellites. Nature **298**, 142-144.

Verbiscer, A. J., and J. Veverka 1992. Mimas: Photometric roughness
and albedo map. Icarus **99**, 63-69.

TABLE 1

Properties of the medium-sized inner Saturnian satellites

Satellite	Semimajor Axis 10^3 km	Orbital Period days	Mean Radius km	Visual Albedo[1]
Mimas	185.5	0.942	199	0.77
Enceladus	238.0	1.370	249	1.04
Tethys	294.7	1.888	530	0.80
Dione	377.4	2.737	560	0.55
Rhea	527.0	4.518	764	0.65

[1]Buratti and Veverka (1984), Table 9.

TABLE 2

Summary of Images: Methane filter (0.889 μm; 50 Å FWHM)

Date (UT; 1995)	Number of Images M E T D R	Mimas	Longitudes Covered Encel.	Tethys	Rhea	Dione	Phase Angle
9 August	46 49 46 14 1	230-276	239-282	20-57	350-6	358-23	3.7
10 August	24 12 24 53 53	266-300	123-145	197-247	64-85	120-155	3.6
11 August	42 23 60 83 59	244-281	50-88	27-79	143-165	251-286	3.5
12 August	11 13 25 41 48	261-268	285-287	220-269	224-245	25-53	3.5

21

TABLE 3

Geometric Albedos

| Satellite | Observed Albedo[1] | | Geometric Albedo | | Adopted |
	Leading	Trailing	Leading	Trailing	Phase Coeff.[2]
Titan	0.086 ± 0.001	0.086 ± 0.001	0.086 ± 0.001	0.086 ± 0.001	0.001
Mimas	-	0.67 ± 0.04	-	0.72 ± 0.06	0.021
Enceladus	0.96 ± 0.03	1.00 ± 0.03	1.02 ± 0.05	1.06 ± 0.05	0.017
Tethys	0.86 ± 0.03	0.72 ± 0.03	0.90 ± 0.05	0.76 ± 0.05	0.016
Dione	0.67 ± 0.03	0.49 ± 0.03	0.72 ± 0.05	0.53 ± 0.05	0.023
Rhea	0.70 ± 0.03	0.60 ± 0.03	0.76 ± 0.05	0.65 ± 0.05	0.024

[1]The albedo derived from the integrated brightness, with no corrections for solar phase effect.
[2]The phase coefficient (β) is in magnitudes/degree.

TABLE 4

Derived Rotational Lightcurve Parameters
(Sinusoidal Fit)

Satellite	Full Amplitude (magnitudes)	θ_0 degrees
Mimas	0.10 ± 0.02	270 ± 10
Enceladus	0.13 ± 0.02	~270
Tethys	0.10 ± 0.02	180 ± 10
Dione	0.40 ± 0.01	180 ± 10
Rhea	0.20 ± 0.03	60 ± 20

FIGURE CAPTIONS

Figure 1. A typical image obtained with the 60-inch telescope on Palomar Mountain, on August 11, 1995 8:24 UT. From left, the satellites are Titan, Dione, Mimas, Enceladus, Tethys, Rhea.

Figure 2. The geometric albedos of the satellites, shown with previous results in the visible region of the spectrum (Buratti and Veverka, 1984). Disk integrated values from our study are shown.

Figure 3. The rotational lightcurve of Mimas. Previous results from Voyager are from Buratti and Veverka (1984) and Verbiscer and Veverka (1992). Both the Voyager and Palomar observations were used in the curve fit.
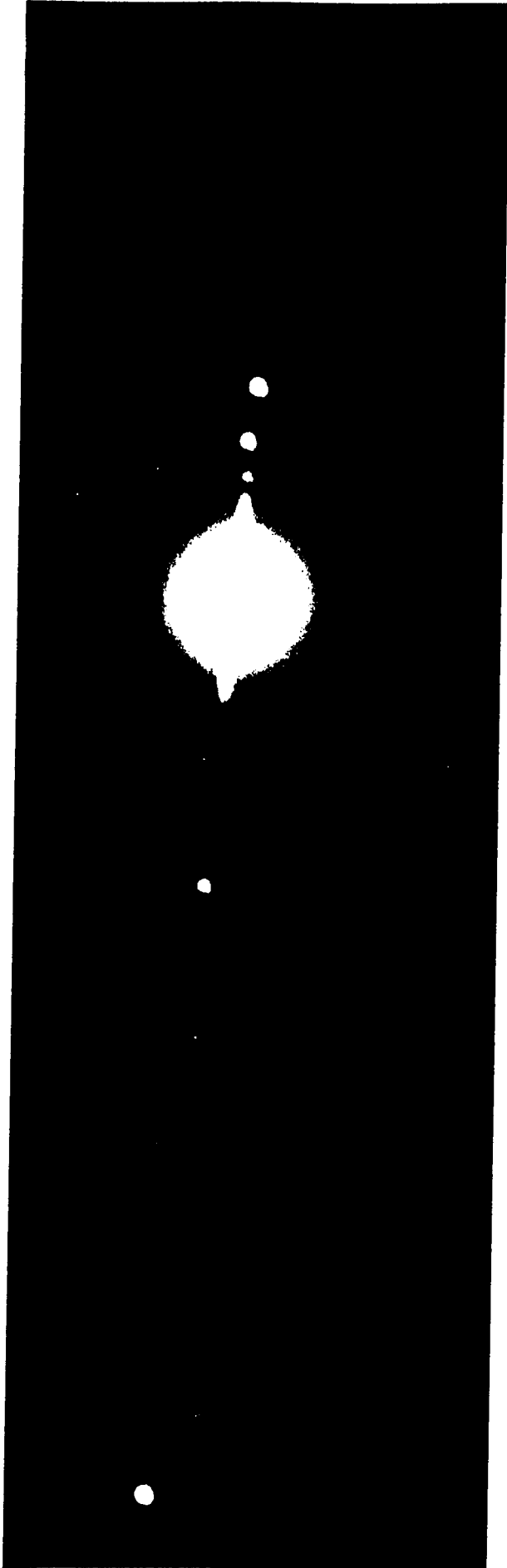
Figure 4. The rotational lightcurve of Enceladus. Unlike the other satellites, the global albedo pattern on Enceladus does not appear to be sinusoidal.

Figure 5. The rotational lightcurve of Tethys, shown with previous results for comparison. Only the Palomar observations were used in the curve fit. The flat portion of the lightcurve for the trailing hemisphere is due to a dark, longitudinally placed feature (Smith et al., 1982).

Figure 6. The rotational lightcurve of Dione, showing a smaller amplitude than the Voyager measurements. Only the Palomar observations were used in the curve fit.

Figure 7. The rotational lightcurve of Rhea, which is in close agreement with previous measurements. Only the Palomar observations were used in the curve fit.
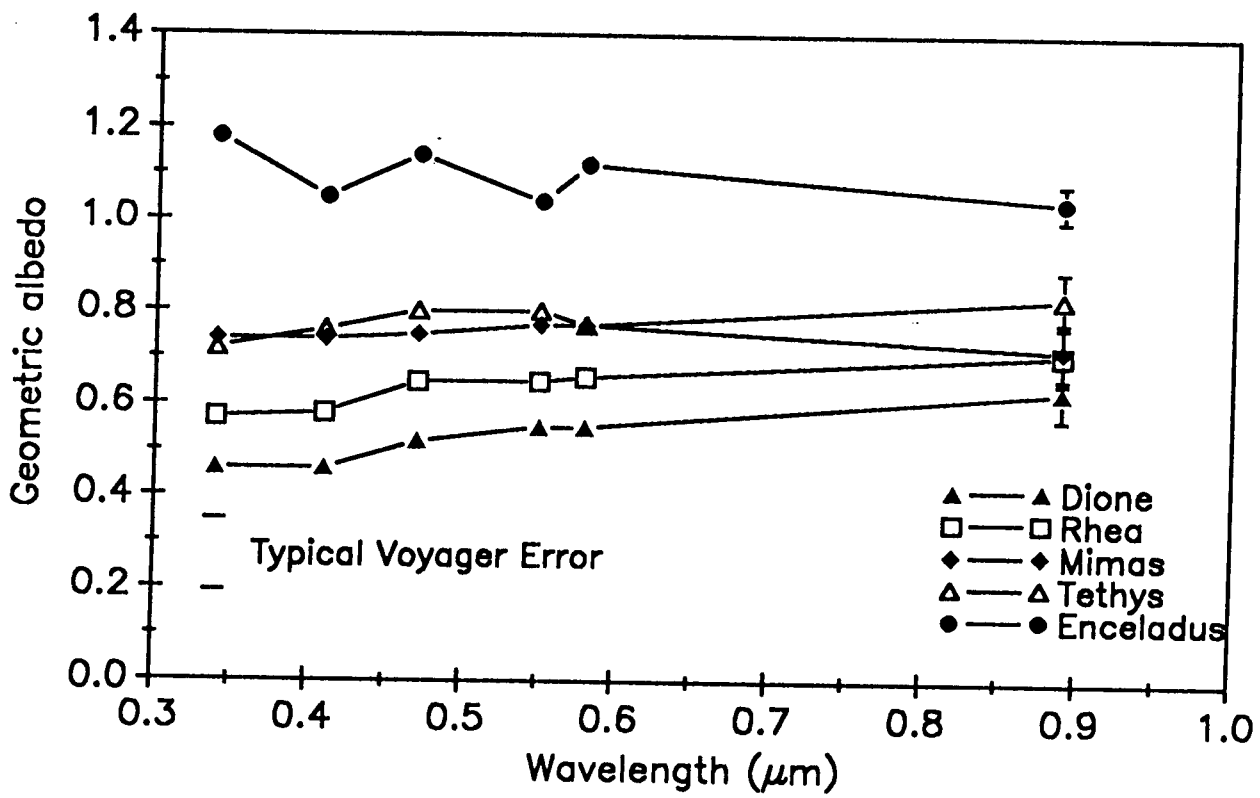
FIG. 2

MIMAS
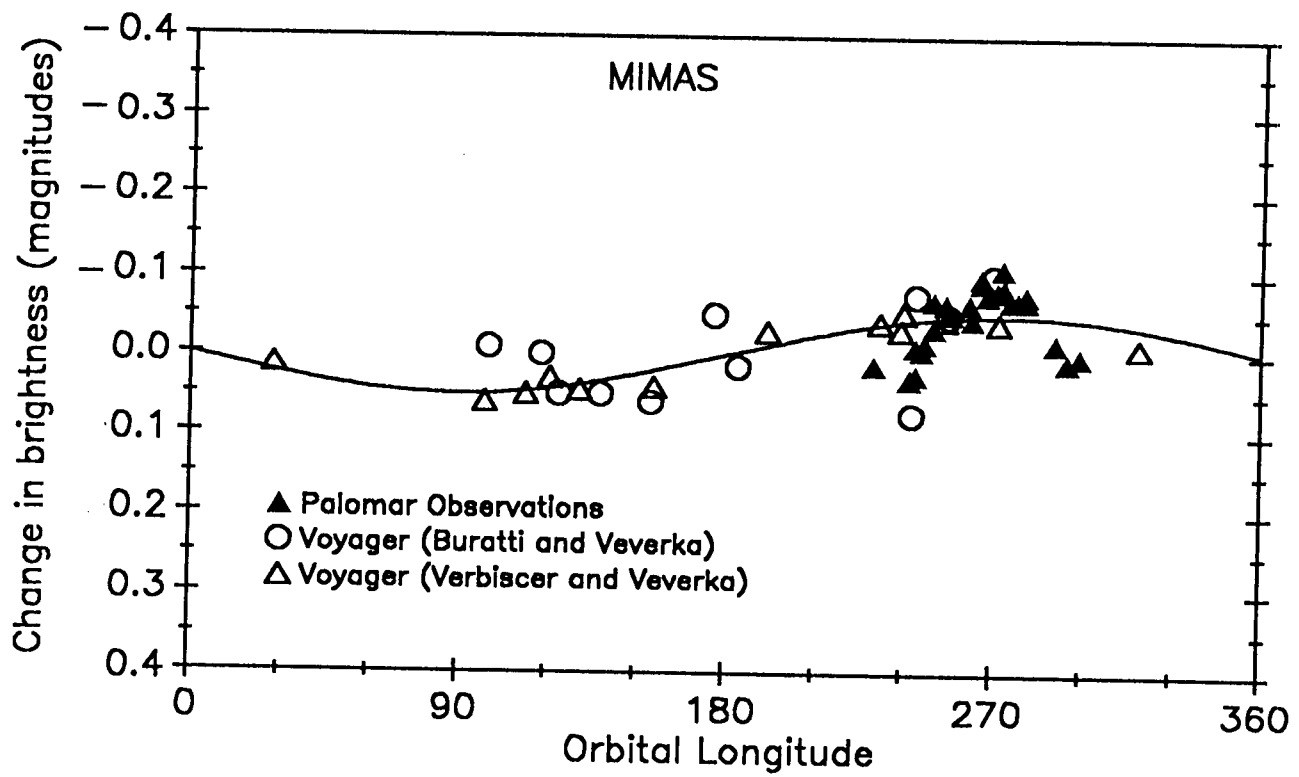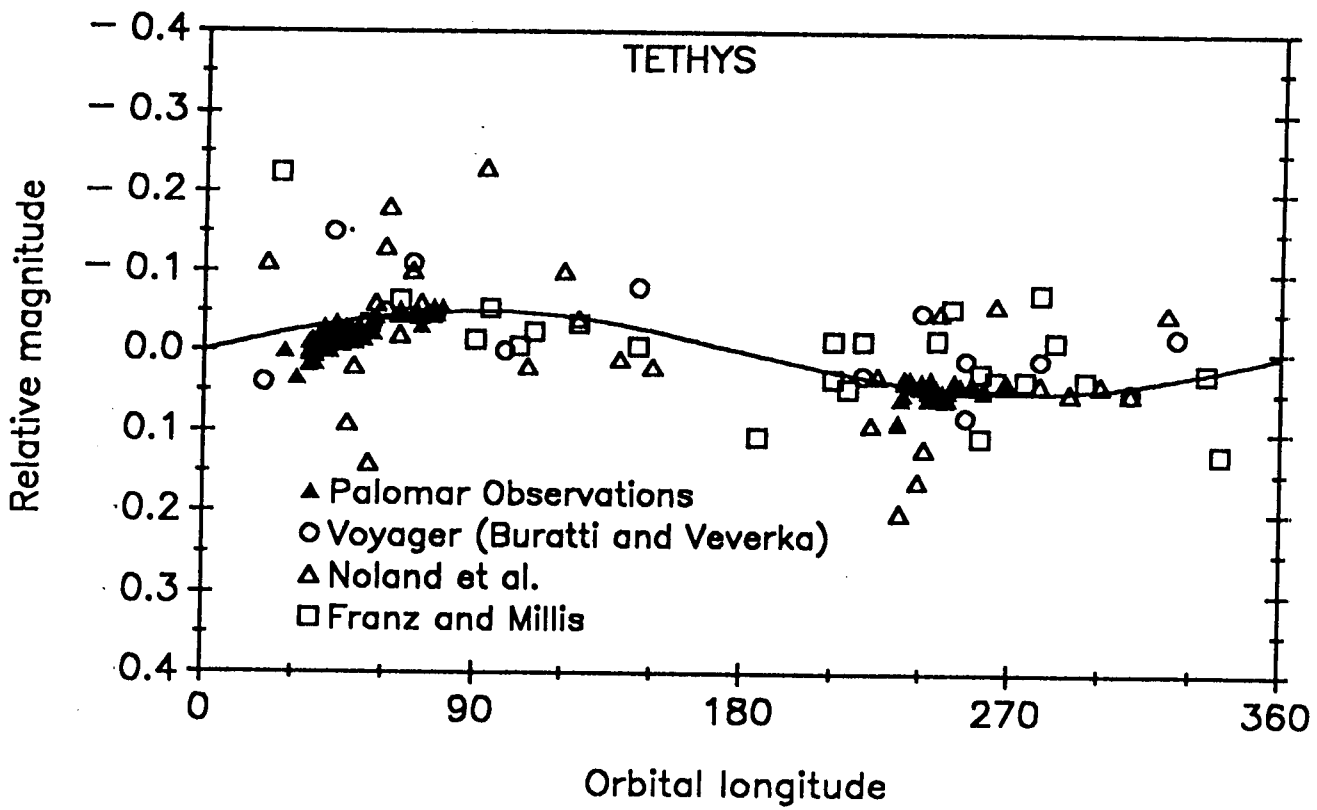
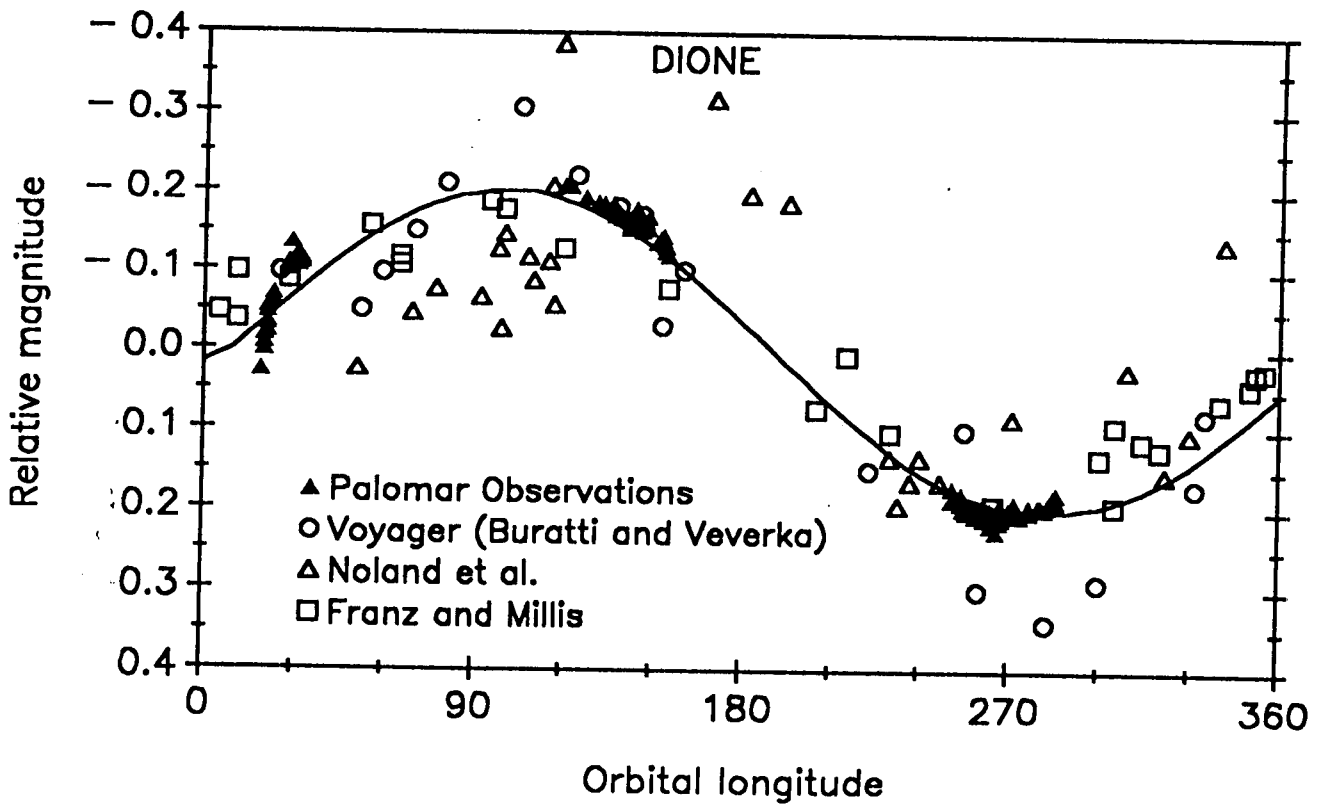▲ Palomar Observations
○ Voyager (Buratti and Veverka)
△ Voyager (Verbiscer and Veverka)

FIG. 3

ENCELADUS

FIG.4

TETHYS

▲ Palomar Observations
○ Voyager (Buratti and Veverka)
△ Noland et al.
□ Franz and Millis

Relative magnitude

Orbital longitude

F/9.5

FIG. 6

RHEA

Relative magnitude

▲ Palomar Observations
○ Voyager (Buratti and Veverka)
△ Noland et al.

Orbital longitude

FIG. 7